A New Approach to Formation and Directed Radiation of Powerful Short Radio Pulses

Yuriy Sirenko, Seil Sautbekov, Nataliya Yashina, and Kostyantyn Sirenko, *Member, IEEE*

***Abstract*— This article details a new method for formation and directional radiation of short high-power electromagnetic (EM) pulses, which is based on a wave analog of the Smith–Purcell effect. The presented device cycles through two stages. At the stage of energy accumulation, a slow wave of an open guiding structure interacts with a periodic chain of storage resonators and excites high-Q free field oscillations in each resonator of this chain. The phase of oscillations inside the storage resonators differs by a constant value, and the amplitude increases with time. At the radiation stage, the chain of storage resonators is opened to radiation (as it usually happens in active compressors of EM pulses), and short powerful pulses burst out into free space in strictly defined directions. The proposed design is considered in detail for the simplest model of a device. The results obtained during its rigorous electrodynamic analysis look rather promising; the continuation of this work can contribute to solving a number of urgent problems of physics and technology of millimeter and submillimeter waves.**

***Index Terms*— Accumulation of electromagnetic energy, active compression of electromagnetic pulses, antenna arrays, boundary conditions, boundary value problems, computational electromagnetics, electromagnetic analysis, electromagnetic radiation, exact absorbing conditions, lamellar gratings, leaky wave antennas, planar dielectric waveguides, powerful short pulses, pulse compression methods, time-domain analysis.**

I. Introduction

ELECTROMAGNETIC (EM) or microwave energy compressors are devices that convert long-duration low-amplitude input pulses into short high-amplitude output. Active compressors achieve it via accumulation of input energy in resonant cavities for (relatively) long time and subsequent much faster release of the accumulated energy [1]–[4], and in passive compressor, input pulse becomes shorter and grows in amplitude as it travels through waveguides with specially designed geometrical and/or material properties [5], [6]. Compressors find their use in many fields where high-power EM pulses are needed: radars, particles accelerators, biomedical applications, EM launch systems, and plasma heating, to name a few [3], [7].

Compressed pulses could reach gigawatt power level [5], and this toughens requirements to compressors' output components, which must be able to handle such power. Reducing distance traveled by high-power pulses, i.e., placing compressors closer to target loads or radiators, could reduce weigh, size, cost, and complexity of devices and also decrease wall loss and distortion of compressed pulses. In [4, Ch. 6] and [8], we presented combined compressor/radiator, which completely eliminates waveguide between compressor and radiator. Also, a possibility to assemble such devices into arrays for directional radiation was demonstrated. However, in order to unleash the full potential of array beam formation and steering, precise timing of excitation and switching (from energy accumulation to release) is required for each array element. In this article, we present a novel design, which enables feeding of all array's compressor/radiator elements simultaneously from a single source. The essence of this design is the realization of a wave analog of the Smith–Purcell effect in a periodic structure, i.e., generation of plane EM waves by means of the interaction of the field of an open waveguide's surface wave with a periodic grating [9]–[12]. Our past studies of this effect resulted in the development of a whole new class of diffraction antennas (also known as leaky-wave antennas) with unique characteristics [4, Ch. 7], [11]–[17]. Deriving inspiration there and in our experience with compressors [3], [4, Ch. 6], [8], [18]–[20], in this work, we present a novel device, which receives and radiates energy in a way similar to diffraction antennas, and accumulates and store it like active compressors of EM pulses. The proposed construction consists of a periodic chain of identical resonators in a vicinity of an open dielectric waveguide. The resonators accumulate and store EM energy during the energy accumulation stage. They are excited by the exponentially decaying part of a slow wave, which is guided by the dielectric waveguide. During the long-lasting excitation, high-Q oscillations are excited inside the resonators, their amplitudes increase with time, and thus, EM energy is accumulated. At the moment when the process of energy accumulation is complete, the excitation ends, the resonators are opened to release the accumulated energy (as it usually happens in active compressors), and short and powerful EM pulses are radiated into free space in strictly defined directions.

We proposed in [3] and [18] and practically implemented in [4], [8], [19], and [20] basic design principles of active compressors of EM pulses on segments of regular waveguides

Manuscript received 30 January 2022; revised 25 April 2022 and 22 May 2022; accepted 7 June 2022. This work was supported in part by the Science Committee of the Ministry of Education and Science of the Republic of Kazakhstan under Grant AP08855557. The review of this article was arranged by Senior Editor R. P. Joshi. *(Corresponding author: Kostyantyn Sirenko.)*

Yuriy Sirenko is with the Department of Diffraction Theory and Diffraction Electronics, O.Ya. Usikov Institute for Radiophysics and Electronics, National Academy of Sciences of Ukraine, 61085 Kharkiv, Ukraine, and also with the Department of Applied Mathematics, V.M. Karazin Kharkiv National University, 61022 Kharkiv, Ukraine (e-mail: yks2002sky@gmail.com).

Seil Sautbekov is with the Department of Physics and Technology, Al-Farabi Kazakh National University, Almaty 050040, Kazakhstan (e-mail: sautbek@mail.ru).

Nataliya Yashina and Kostyantyn Sirenko are with the Department of Diffraction Theory and Diffraction Electronics, O.Ya. Usikov Institute for Radiophysics and Electronics, National Academy of Sciences of Ukraine, 61085 Kharkiv, Ukraine (e-mail: yashinanp@gmail.com; k.sirenko@gmail.com).

Color versions of one or more figures in this article are available at https://doi.org/10.1109/TPS.2022.3184268.

Digital Object Identifier 10.1109/TPS.2022.3184268

and open compact resonators. There, practically for the first time, energy accumulation and release processes were accurately modeled in time domain from the very beginning of excitation to the end of energy release; important dynamic characteristics of storage resonators were rigorously calculated; switches (locks) allowing efficient, quick, and well-timed release of the accumulated energy into output waveguides or free space have been synthesized. The obtained methodological conclusion says that the design of compressors with required characteristics is possible only after thorough and accurate mathematical modeling and simulation. Such preliminary semianalytical intellectual work simplifies significantly the optimization process and makes it more cost-effective. Naturally, compressors are resonant devices, and thus, it is a challenging task to simulate them accurately and efficiently in the time domain. For numerical simulations in this article, we use the method of exact absorbing condition (EAC-method) [4, Ch. 5], [21]–[26]. The EAC-method is well adapted for problems of analysis and synthesis of active compressors and their functional units [3], [4], [8], [18]–[20]. It is fast and does not distort the physics of processes under study [4], [23]–[25]. Its computational schemes are stable and virtually with no additional errors run through tens of millions of time steps, the duration common for problems under consideration [3], [4], [18]. It has proved itself to be more accurate and efficient than other popular methods for truncation of computation domains that exploit approximate or heuristic absorbing conditions [22], [26].

This article is organized as follows. Section II presents the mathematical model under consideration, and geometry and operating principles of the proposed construction. Section III details the design steps for the proof-of-concept device and suggests possible measures to improve its characteristics. Section IV demonstrates that suggestions from Section III indeed grade up characteristics of the device. The Appendix details the device's characteristics under study.

We use SI, the International System of Units, for all physical parameters except the time t that is the product of the natural time and the velocity of light in vacuum, and thus, t is measured in meters. In this article, all dimensions are omitted. According to SI, all geometrical parameters (a, b, c, and so on) are given in meters. However, there are obviously no obstacles to scale the results to any other geometrically similar structure. For the sake of convenience, as a frequency parameter, we use wavenumber since it remains invariable under the aforementioned normalization of time.

II. Model Problem and the Object of Interest

This section introduces rigorous mathematical formulation of a model problem describing the EM behavior of the construction of interest (Section II-A), and details the geometry and principle of operation of the device under study (Section II-B).

A. Mathematical Problem

Consider the object shown in Fig. 1, it is a periodic structure in the vicinity of a dielectric waveguide. For now, we note that

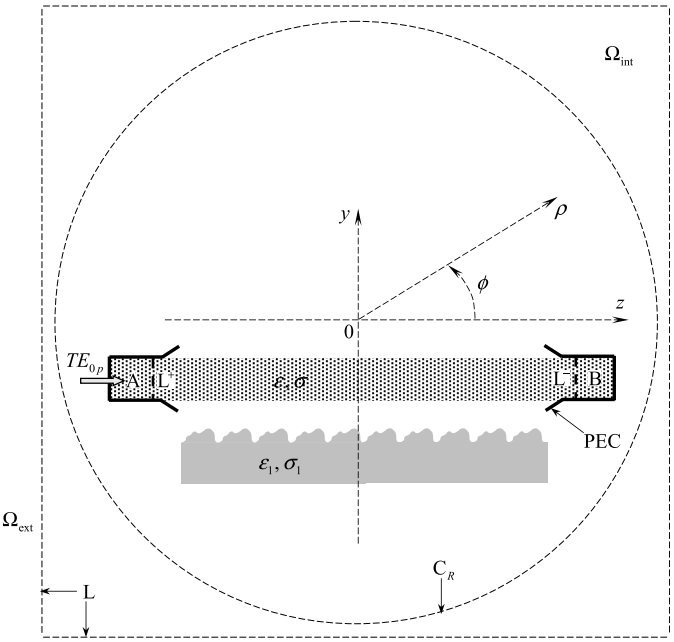

Fig. 1. Geometry of the model problem (1), section by the plane $x = \text{const}$.

it is uniform along the x-axis and will discuss its geometry and material features in Section II-B. Let this object be excited by eigen TE_{0p}-wave $V_p(g,t) = v_p(z,t)\mu_p(y)$, $g \in \text{A}$ of the plane-parallel waveguide A through the virtual boundary L$^+$. Under this conditions, space-time transformations of TE_0-waves ($E_y = E_z = H_x \equiv 0$ and $\partial_x = 0$) by the object of interest are described by the following scalar initial boundary value problem [3], [4]:

$$\begin{cases} \left[-\varepsilon(g)\partial_t^2 - \eta_0 P + \partial_y^2 + \partial_z^2\right]E_x(g,t) = 0; \\ \qquad g \in \Omega_{\text{int}}, \quad t > 0 \\ E_x(g,0) = 0, \quad \partial_t E_x(g,t)|_{t=0} = 0; \quad g \in \overline{\Omega_{\text{int}}} \\ D^-[E_x(g,t)]\big|_{g\in \text{L}^-} = 0,\ D^+\left[E_x(g,t) - V_p(g,t)\right]\big|_{g\in \text{L}^+} = 0, \\ D[E_x(g,t)]|_{g\in \text{L}} = 0; \quad t \geq 0. \end{cases} \tag{1}$$

Here, $P[E_x] \equiv \partial_t[\sigma(g,t)E_x(g,t)]$; $\mathbf{E}(q,t) = \{E_x, E_y, E_z\}$ and $\mathbf{H}(q,t) = \{H_x, H_y, H_z\}$ are the electric and magnetic field vectors, respectively; $q = \{x,y,z\}$ and $g = \{y,z\}$; the piecewise-constant functions (of the argument g) $\sigma(g,t) \geq 0$ and $\varepsilon(g) > 0$ are the specific conductivity and relative permittivity of nonmagnetic elements; and η_0 is the impedance of free space. The conventional assumptions of the properties of tangential field components and the smoothness of surfaces of perfect electric conductors (PECs) and dielectric elements are assumed to be fulfilled.

The computation domain Ω_{int} in (1) is the part of the plane $y0z$ bounded by the PEC surfaces together with the virtual boundaries L$^\pm$ (input and output ports in the cross sections of the virtual [25] waveguides A and B) and the rectangular virtual boundary L, which separates Ω_{int} and the free-space domain Ω_{ext}. The circular virtual boundary C$_R$, which has radius R and center at the beginning of the Cartesian (y,z) and

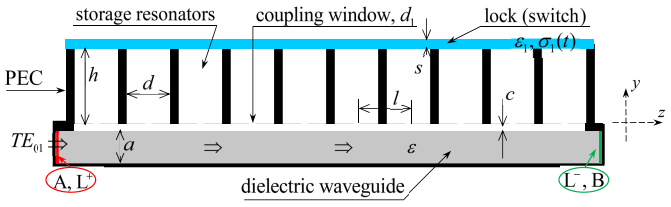

Fig. 2. Geometry of the device, section by the plane $x = \text{const}$. Proportions preserved.

polar (ρ, ϕ) coordinates, covers all scattering inhomogeneities of the domain Ω_{int} and is completely contained in it.

The boundary conditions for $L^{\pm}$ and L, namely, EACs $D^{\pm}[\ldots]$ and $D[\ldots]$, are explained in the Appendix.

B. Geometry and Operating Principle of the Device

The Smith–Purcell effect is generation of homogeneous plane EM waves when a plane, density-modulated electron flow moves at a constant speed over a 1-D periodic grating. The number of waves, their wavelength, and directions are defined by parameters of the electron beam and the grating's period. The field of plane EM waves is generated by the eigenfield of the electron flow [9], [10]. Studies of relevant phenomena have enriched modern physics and made possible the creation of unique devices. Also, it laid the foundations for mathematical modeling of diffraction radiation, which in turn allowed to widen the range of phenomena under study with the so-called wave analog of the Smith–Purcell effect. In this case, the part of the eigenfield of the electron flow is played by the field of an inhomogeneous plane wave or the field of a surface wave guided by an open waveguide. In the case of H-polarization of the field, these waves generate the same field as the eigenfield of a plane, density-modulated electron flow [12], [24]. In this article, the wave analog of the coherent Smith–Purcell radiation is realized via the diffraction of a surface wave of an open dielectric waveguide by a grating formed by an array of storage resonators.

Thus, the device of interest consists of a periodic structure in the vicinity of a dielectric waveguide, namely, a periodic chain (array) of identical storage resonators located near an open planar dielectric waveguide, see Fig. 2. The storage resonators are excited through the cutoff coupling windows by the exponentially decaying part of a slow wave, which is guided by the dielectric waveguide. The storage resonators accumulate and store EM energy as high-Q eigen oscillations, which are excited if the frequency of excitation coincides with the real part of one of the eigenfrequencies of the resonators. The amplitudes of these oscillations continuously grow during the excitation, and the phase differs by a constant value determined by the moderating coefficient of the primary wave and the resonator chain's period. When the energy accumulation ends, the resonators are opened, and the accumulated energy is released in strictly defined directions as short and powerful EM radio pulses, which are analogs of spatial harmonics of a periodic structure [11], [22], [24].

This construction allows to radiate the accumulated energy in a way resembling phased array antennas or some diffraction antennas (which are also called leaky-wave antennas). However, in contrast with the former, elements of periodic structure (storage resonators) are excited not individually but simultaneously from one common source of energy, namely, the field of a surface wave of a planar dielectric waveguide. This excitation method is another similarity between the presented device and diffraction antennas [4, Ch. 7], [11]–[17]. However, in contrast with them, there is energy accumulation stage between excitation and radiation. In other words, the radiation is "delayed" until the end of energy accumulation in storage resonators.

The main electrodynamic characteristics of the device are determined by the parameters of its functional elements (see Fig. 2) which are listed next.

1) Periodic chain of storage resonators has period l. Each storage resonator is a segment of plane-parallel waveguide with the width d and height h, and they have PEC walls. The storage resonators are coupled with the field of a wave guided by the dielectric waveguide through the cutoff coupling windows (with the width d_1) in the thin (only 0.02 thick) wall located at the aiming distance c from the dielectric waveguide.
2) Planar dielectric ($\varepsilon = \text{const} > 1$, $\sigma = 0$) waveguide has the width a. It supports propagation of a slow surface wave with the frequency-dependent moderating coefficient $\gamma(k)$. This wave is fed through the virtual boundary L^+ by TE_{01}-wave of the virtual waveguide A and outgoes through the virtual boundary L^- into the virtual waveguide B. Uniform phase shift between the storage resonators is ensured by the absence of phase distortions in the excitation wave [constant moderating coefficient $\gamma(k)$] throughout the whole length of its interaction with the chain of resonators [11], [14].
3) Dielectric ($\varepsilon_1 = \text{const} \geq 1$) screen on the top of the storage resonators has thickness s. This screen locks the chain of resonators when the device operates in the energy accumulation mode and quickly unlocks the device when switched to the radiation mode. In the energy accumulation mode, the conductivity $\sigma_1(t)$ of the screen is high, and this makes it nontransparent for EM waves and therefore locks the storage resonators. In contrast, in the radiation mode, $\sigma_1(t)$ is low, and thus, the energy accumulated in the storage resonators could be released. The switching between accumulation and radiation modes is achieved via quickly changing $\sigma_1(t)$.

III. Preliminary Analysis

Let us consider the device shown in Fig. 2 with the following values of parameters: $\varepsilon = 2.1$ (corresponds to that of Teflon), $a = 1.0$, $d = 1.5$, $h = 2.0$, $l = 1.8$, $d_1 = 0.22$, $c = 0$, $s = 0.3$, $\varepsilon_1 = 1$, and $\sigma_1 = 5.7 \cdot 10^4$ (energy accumulation mode), see Section II-B for the description of these parameters. Let this device be excited by TE_{01}-pulse

$$V_1(g,t): \quad v_1\big(z: g \in L^+, t\big) = 4\sin\big[\Delta k\big(t-\tilde{T}\big)\big]\big(t-\tilde{T}\big)^{-1} \times \cos\big[\tilde{k}\big(t-\tilde{T}\big)\big]\chi\big(\tilde{T}-t\big). \quad (2)$$

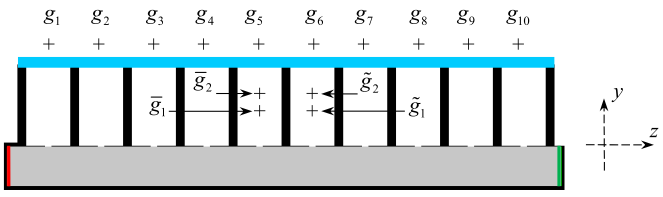

Fig. 3. Geometry of the device with observation points.

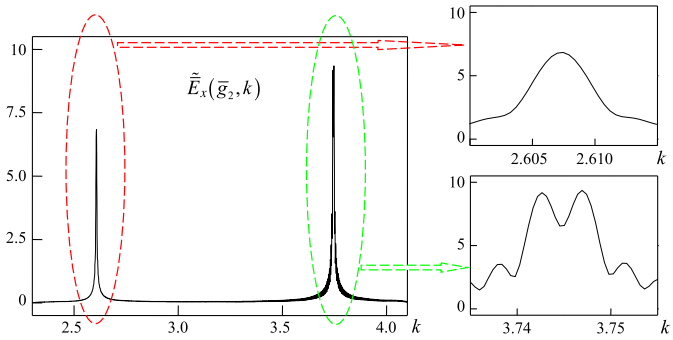

Fig. 4. Real parts of complex wavenumbers defining eigenfrequencies of the storage resonators.

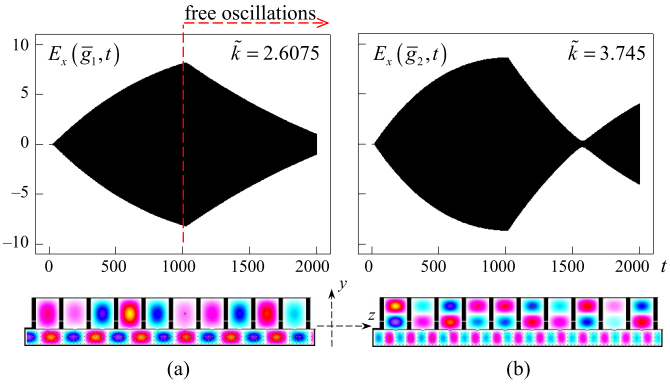

Fig. 5. Excitation of the device by the signal (3) with (a) $\tilde{k}=2.6075$ and (b) $\tilde{k}=3.745$: time signatures of $E_x(g,t)$ at the points $\bar{g}_1$ and $\bar{g}_2$, and field patterns (E_x component) at the time moment $t=145$.

Here, $\chi(\ldots)$ is the Heaviside step function, $\tilde{k}=3.2$ is the wavenumber defining the central frequency of the signal, $\tilde{T}=50$ and $\bar{T}=100$ are the signal's delay and duration, respectively, and $\Delta k=0.9$ sets the range of wavenumbers covered by the signal (and thus defines its frequency band): $\tilde{k}-\Delta k\le k\le\tilde{k}+\Delta k$ ($2.3\le k\le 4.1$) [3], [22]. We would like to note here that we consider TE_{0n}-waves only in this article. It is preferred as utilization of this kind of waves usually leads to reduced heat loss in walls of real-world devices. However, there are no principal differences from the case of *TM*-waves, and similar discussion is valid also for compressors utilizing *TM*-waves [8], [18].

Let $k_n=n\pi/a(\varepsilon)^{1/2}$, $n=1,2,\ldots$, denote cutoff wavenumbers of monochromatic TE_{0n}-waves in a plane-parallel waveguide of the width a filled with a material with permittivity ε (i.e., k_n is the lowest wavenumber for which waves propagate without attenuation). For k within the excitation's band ($2.3\le k\le 4.1$), only TE_{01}-waves propagate in waveguides A and B without attenuation, as the cutoff wavenumbers there are $k_1\approx 2.17$ and $k_2\approx 4.34$. The storage resonators are formed by segments of plane-parallel waveguides with the cutoff wavenumbers $k_1\approx 2.09$ and $k_2\approx 4.19$, so again, only TE_{01}-waves can propagate without attenuation there. The coupling windows remain beyond cutoff up to $k\approx 14.28$.

Despite the novel compressor's design, its development follows the standard design scheme for EM energy compressors, which is detailed in [3] and [18]. First, the function $E_x(g,t)$ is computed for $0<t\le T=2000$ (well after the source is turned off at $t=\bar{T}=100$) at the points $\bar{g}_1$ and $\bar{g}_2$, which belong to the axis of symmetry of one of the storage resonators, see Fig. 3. Then, $\tilde{\bar{E}}_x(g,k)$ is calculated as a result of applying the transform (A2) to $E_x(g,t)\chi(t-\bar{T})\chi(T-t)$ [the transform (A2) is defined in the Appendix]. Peaks of the curves $\tilde{\bar{E}}_x(\bar{g}_j,k)$ point to real parts of complex wavenumbers $\bar{k}=\mathrm{Re}\bar{k}+i\mathrm{Im}\bar{k}$ ($\mathrm{Im}\bar{k}<0$) defining eigenfrequencies of the storage resonators [3], [22], [27]–[29]. There are only two of them ($\mathrm{Re}\bar{k}_1\approx 2.6075$ and $\mathrm{Re}\bar{k}_2\approx 3.745$) within the band of interest $2.3\le\mathrm{Re}\bar{k}\le 4.1$, see Fig. 4. For the selected values of h and d, they correspond to $H_{0,1,1}$- and $H_{0,1,2}$-oscillations in the storage resonators (Fig. 5, lower fragments). The points $\bar{g}_1$ and $\bar{g}_2$ almost exactly coincide with antinodes of these oscillations, see Fig. 3, and the lower fragments of Fig. 5. The obtained values of $\mathrm{Re}\bar{k}_j$ determine resonant frequencies at which the accumulation of energy in the storage resonators is possible under long-duration excitation by the corresponding monochromatic signals. Thus, these frequencies are candidates for the device's working frequency [3], [4], [18].

Repeating this procedure for the points $\tilde{g}_j$ in one of the neighboring resonators (see Fig. 3), the function $\Phi_0(k)=[\arg\tilde{E}_x(\tilde{g}_j,k)-\arg\tilde{E}_x(\bar{g}_j,k)]l^{-1}$ is computed. It characterizes the phase shift of the field along the chain of resonators (which could also be considered as finite grating) and determines the number and spatial orientation of plane waves traveling away from the device into free space [8], [11], [22], [24], [30]–[33]. Assuming qualitatively identical role of spatial harmonics of infinite and finite gratings in the formation of radiated field, we conclude that the main lobes of the radiation pattern are oriented approximately in the directions $\phi_n=90^\circ-\arcsin(\Phi_n/k)$, where $\Phi_n=\Phi_0+2\pi n/l$, $n:\ k>|\Phi_n|$ [4], [11]. The angles ϕ are measured counterclockwise from the axis z, see Fig. 1. In our case, we have the following values: for the first candidate frequency, $\Phi_0(\mathrm{Re}\bar{k}_1)=1.98$, and for the second candidate frequency, $\Phi_0(\mathrm{Re}\bar{k}_2)=0.95$. Therefore, when the device is opened for radiation, the radiation mainly goes in the directions $\phi\approx 41^\circ$ and $\phi\approx 125^\circ$ for the first candidate frequency and in the directions $\phi\approx 75^\circ$ and $\phi\approx 133^\circ$ for the second candidate frequency. These directions correspond to the fundamental (zeroth) and the minus first spatial harmonics of infinite grating.

Now, we determine the field configuration and the quality factor $Q=\mathrm{Re}\bar{k}/2|\mathrm{Im}\bar{k}|$ of the oscillations on the candidate frequencies. For it, the device is excited with the narrowband signal

$$V_1(g,t):\quad v_1\big(z:g\in\mathrm{L}^+,t\big)=P(t)\cos\big[\tilde{k}\big(t-\tilde{T}\big)\big]. \qquad (3)$$

Here, $\tilde{k} = \mathrm{Re}\bar{k}_j$ is the wavenumber defining the central frequency of the signal, $\tilde{T} = 0.5$ is the delay, and $P(t)$: $0.1 - 5 - 995 - 1000$ ($P(t)$: $T_1 - T_2 - T_3 - T_4$ is a trapezoidal envelope, which equals one for $T_2 < t < T_3$ and is zero for $t < T_1$ and $t > T_4 = \bar{T}$). After switching OFF the source ($t > 1000$), the field of each storage resonator is dominated by the oscillation with complex wavenumber $\bar{k}$. Its real part is set by $\tilde{k}$ of the excitation. In the case of the first candidate frequency ($\tilde{k} = \mathrm{Re}\bar{k}_1$), the behavior of the module of the envelope $A\exp[\mathrm{Im}\bar{k}_1(t-\bar{T})]$ of the function $E_x(\bar{g}_1, t)\chi(t-\bar{T})\chi(T-t)$, $\bar{T} < t \le T = 2000$, uniquely determines the imaginary part's value $\mathrm{Im}\bar{k}_1 \approx -0.00198$, see Fig. 5(a) [3], [18], [22], [27]–[39]. In the case of the second candidate frequency ($\tilde{k} = \mathrm{Re}\bar{k}_2$), this technique does not work: in the free oscillation mode ($t > 1000$), $E_x(\bar{g}_2, t)$ first decreases exponentially and then begins to grow again, see Fig. 5(b). This unusual behavior is explained by the fact that each storage resonator is coupled with the neighboring ones. The level of this coupling is determined by the size of coupling window and the frequency. The higher this coupling is, the more the basic oscillation gets distorted by oscillations of the same type (but shifted in phase and with lower amplitudes) imposed by the neighboring resonators. This, in particular, leads to the splitting of the resonance peak of $\tilde{\bar{E}}_x(\bar{g}_2, k)$ associated with the corresponding oscillation. This splitting becomes noticeable only with a significant zoom into the small vicinity of the point $k = \mathrm{Re}\bar{k}_2$, see Fig. 4. Such behavior excludes the second candidate frequency from consideration for the working frequency. The further analysis is focused on $H_{0,1,1}$-oscillation in the storage resonators, whose complex wavenumber is $\bar{k}_1 = 2.6075 - i0.00198$.

Now, let $\sigma_1(t) = 5.7 \cdot 10^4$ for $0 \le t \le 3000$ (energy accumulation mode), $\sigma_1(t) = 0$ for $t \ge 3001$ (radiation mode), and $\sigma_1(t)$ is continuous and decreases exponentially on the interval $3000 \le t \le 3001$. The device is excited with the long quasi-monochromatic signal (3) with the following parameters: $\tilde{k} = \mathrm{Re}\bar{k}_1$, $\tilde{T} = 0.5$, and $P(t)$: $0.1 - 5 - 2995 - 3000$. Characteristics of the device operating in the energy accumulation mode ($0 \le t \le t_{\mathrm{accum}} = 3000$) are presented in Figs. 6 and 7. Fig. 6(a) and (b) plot time signatures of the amplitudes of the waves transmitted through the virtual boundaries L^- and L^+ into the virtual waveguides B and A, respectively. See the Appendix for definitions of the amplitudes $u_{11}^{\pm}(z, t)$. Fig. 6(a) and 6(b) allow observation of these (wasteful) waves' evolution in time as the energy accumulates in the storage resonators. Fig. 6(c) shows how the field strength $E_x(\bar{g}_1, t)$ grows in the storage resonator during the energy accumulation. It worth noting that for the considered device, $E_x(\bar{g}_1, t)$ reaches its maximum at the moment of time $t = 2140$ [marked in Fig. 6(c)] and then gradually decreases. This means that after this moment, the device does not accumulate the input energy anymore and there is no point to continue excitation. Fig. 6 gives a fairly complete picture of all space-time transformations of the field during long and constant pumping of the device by the narrowband signal whose central frequency almost exactly coincides with the first candidate frequency. With an absolutely

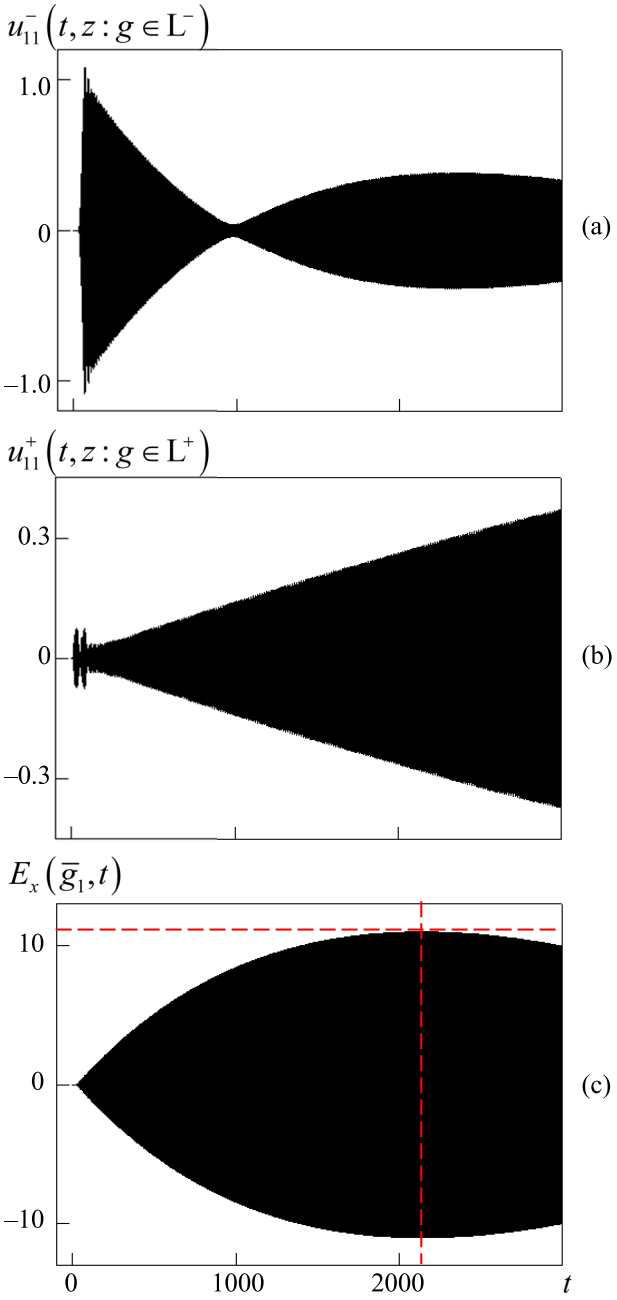

Fig. 6. Energy accumulation mode. Amplitudes of the waves (a) transmitted into B and (b) reflected into A. (c) Field strength at the antinode of the working oscillation.

exact coincidence (and with a very weak coupling between the storage resonators), there would be no decrease of $E_x(\bar{g}_1, t)$ for $t > 2140$, see Fig. 6(c) [3], [4], [18]. The curves in Fig. 7(a) plot the input energy against the time t ($W_{\mathrm{inc,\,L^+}}(t; 0)$) and its (wasteful) distribution between the waveguides A and B ($W_{\mathrm{rad,\,L^+}}(t; 0)$ and $W_{\mathrm{rad,\,L^-}}(t; 0)$, see the Appendix for definitions). These values allow to calculate the energy accumulated in the storage resonators by the moment of time t: $W_{\mathrm{accum}}(t; 0) = W_{\mathrm{inc,\,L^+}}(t; 0) - W_{\mathrm{rad,\,L^+}}(t; 0) - W_{\mathrm{rad,\,L^-}}(t; 0)$. The main characteristic of the accumulation mode is the accumulation efficiency (as a function of time t)

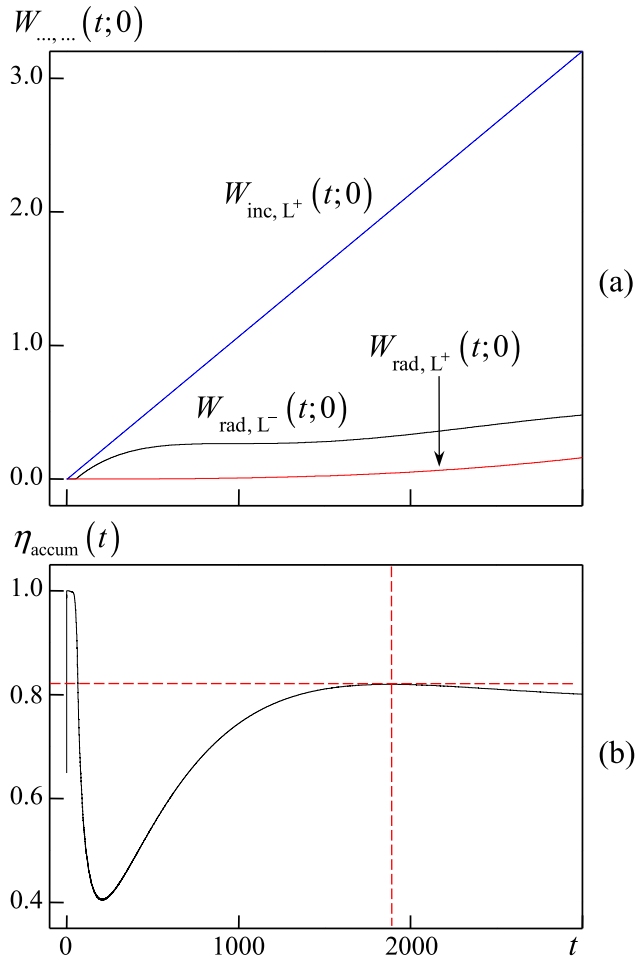

Fig. 7. Energy accumulation mode. (a) Input energy and its distribution between A and B. (b) Accumulation efficiency as functions of time.

$\eta_{\text{accum}}(t) = W_{\text{accum}}(t;0)/W_{\text{inc, L}^+}(t;0)$, and it is plotted in Fig. 7(b). It allows to determine the moment of time when the efficiency of the device reaches its maximum. In general, this is the right moment to switch from the energy accumulation mode to the radiation mode. We would like to note here that the maximum values of $\eta_{\text{accum}}(t)$ in the case under consideration are not inferior to the ones obtained for direct-flow waveguide compressors in [3], [4], [8], and [18].

Within the interval $t_{\text{accum}} = 3000 \le t \le 3001 = t_{\text{rad}}$, the device switches from the energy accumulation mode to the radiation mode, the dielectric screen covering the chain of storage resonators becomes transparent for EM waves, and the energy accumulated in the storage resonators is released into free space as a short powerful radio pulse. Fig. 8 details the characteristics of this process. The time signatures of $E_x(g,t)$ recorded at the points g_1–g_{10} located on the line $y = \text{const}$ with the distance l between each other (see Fig. 3) allow us to estimate the effective duration of the radiated pulse $\Delta t_{\text{effect}} \approx 25$ and the degree of compression (compression ratio) $\beta = t_{\text{accum}}/\Delta t_{\text{effect}} \approx 120$. The ratio of the energies in the radiated pulse ($W_{\text{rad, L}}(3050; t_{\text{rad}}) \approx 2.55$) and in the input signal ($W_{\text{inc, L}^+}(t_{\text{accum}}; 0) \approx 3.25$) determines the radiation efficiency of the device $\eta_{\text{rad}} = W_{\text{rad, L}}(3050; t_{\text{rad}})/W_{\text{inc, L}^+}(t_{\text{accum}}; 0) \approx 0.78$ and its power amplification factor $\zeta = \beta \cdot \eta_{\text{rad}} \approx 93.6$.

The energy characteristics of the considered device are satisfactory. The obtained orientations of the far-field radiation pattern's lobes [$\phi_1 \approx 42°$ and $\phi_2 = \bar{\phi} \approx 123°$, see Fig. 8(b)] perfectly match our theoretical predictions from the beginning of this section ($\phi \approx 41°$ and $\phi \approx 125°$). At the same time, the radiation pattern [see Fig. 8(b)] has undesirable features, namely, two beams, large width of the main lobes, and high level of sidelobes. Naturally, they should be eliminated when designing real-world devices. In Section IV, we demonstrate the possibility of improvement and optimization of the radiation characteristics. However, first, we discuss the main shortcomings of the design, what causes them and how to treat them.

The first noted drawback is the splitting of higher resonant frequency due to the coupling of neighboring storage resonators. The negative consequences of this coupling can be minimized by increasing the aiming distance c and reducing the size of coupling window d_1.

The two-lobe pattern is addressed via tuning the period l of the resonator's chain and the moderating coefficient $\gamma(k)$ of the surface wave of planar dielectric waveguide [4], [14].

The width of the main lobe and the level of sidelobes could be decreased via the formation of required (in particular, uniform) amplitude distribution of the field over the emitting aperture [14]. Apparently, it is not the case for the considered device, and Fig. 8(a) clearly shows more than an order of magnitude difference between amplitudes of the waves radiated from the outermost storage resonators. It is addressed via turning the aiming distance c into a function of the coordinate z, $c(z)$, so that the storage resonators would receive approximately equal shares of the input energy.

IV. Improving Characteristics of the Device

In this section, we implement the suggested modifications and demonstrate that it indeed improves the device's characteristics. For it, we change a bit the geometry of storage resonators ($d = 0.98$ and $l = 1.0$), reduce the size of coupling windows ($d_1 = 0.14$), and keep the other measurements the same ($a = 1.0$ and $h = 2.0$). The storage resonators and the coupling windows are filled now with the same material as the dielectric waveguide, and it is Teflon with $\varepsilon = 2.1$. The aiming distance is set now by the linear function $c(z)$, and it varies from $c = 0.1$ at the exit from the virtual waveguide A (virtual boundary L^+) to $c = 0$ at the entrance to the virtual waveguide B (virtual boundary L^-), see Fig. 9. The dielectric screen covering the chain of storage resonators is not flat but periodic now. It is made of isosceles triangles with the height and base of 0.98 (see Fig. 9). Its constitutive parameters are: $\varepsilon_1 = 2.1$ (the same as inside the storage resonators), $\sigma_1(t) = 5.7 \cdot 10^4$ for the energy accumulation mode, and $\sigma_1(t) = 0$ for the radiation mode.

Let this device be excited by TE_{01}-pulse (2) whose parameters are set as $\tilde{k} = 3.3$, $\Delta k = 1.0$, $\tilde{T} = 50$, and $\bar{T} = 100$. This pulse occupies the band $2.3 < k < 4.3$. For k within this band, similar to Section III, the storage resonators and

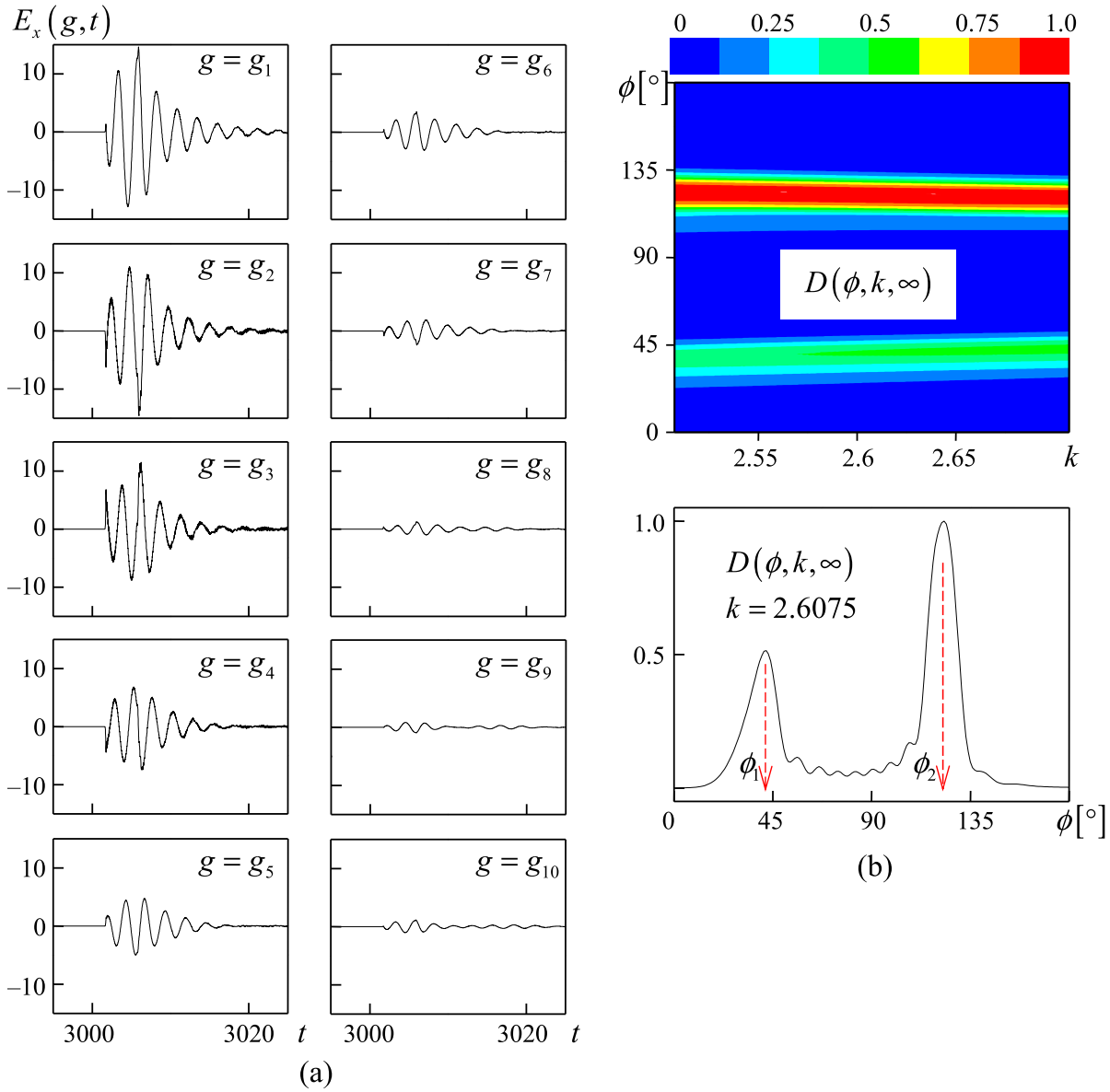

Fig. 8. (a) Time signatures of the radiated pulses at the points g_1–g_{10}. (b) Far-field radiation patterns for the band and for the wavenumber $k = 2.6075$; $\phi_1 \approx 42°$, and $\phi_2 = \tilde{\phi} \approx 123°$.

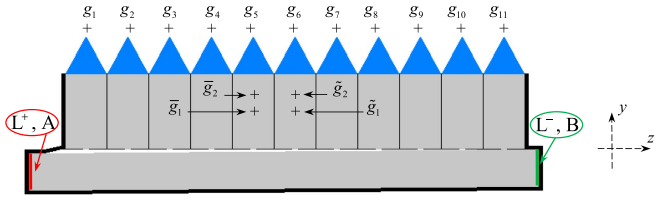

Fig. 9. Geometry with observation points.

waveguides A and B support only TE_{01}-waves, the coupling windows remain beyond cutoff up to $k \approx 15.48$.

Following the steps outlined in Section III, we find resonant frequencies that allow energy accumulation in the storage resonators. For it, the function $E_x(g,t)$ is computed for $0 < t \le T = 2000$ (well after the source is switched OFF at $t = \bar{T} = 100$) at the point $\bar{g}_2$, see Fig. 9. Peaks of $\tilde{\bar{E}}_x(\bar{g}_2,k)$, which is the result of the transform (A2) applied to $E_x(\bar{g}_2,t)\chi(t-\bar{T})\chi(T-t)$, suggest that there are three eigenfrequencies within the band of interest. The real parts of corresponding wavenumbers are $\mathrm{Re}\bar{k}_1 \approx 2.459$, $\mathrm{Re}\bar{k}_2 \approx 3.0835$, and $\mathrm{Re}\bar{k}_3 \approx 3.9075$, see Fig. 10. For the selected values of h and d, they correspond to $H_{0,1,1}$-, $H_{0,1,2}$-, and $H_{0,1,3}$-oscillations in the storage resonators (Fig. 11, upper fragment). As the device's working frequency, let us choose the one with $\mathrm{Re}\bar{k}_3 \approx 3.9075$ since the field with higher frequency (larger wavenumber) should leave the storage resonators faster when the device switches to the radiation mode.

To confirm the improvement of the radiation characteristics, we compute the function $\Phi_0(k) = [\arg \tilde{E}_x(\tilde{g}_j,k) - \arg \tilde{E}_x(\bar{g}_j,k)]l^{-1}$, which characterizes the phase shift of the field along the chain of resonators. For the working frequency, it is $\Phi_0(\mathrm{Re}\bar{k}_3) = 4.85$. Thus, in the radiation mode, the radiation mainly goes in one direction only, $\phi \approx 111.5°$. This direction corresponds to the

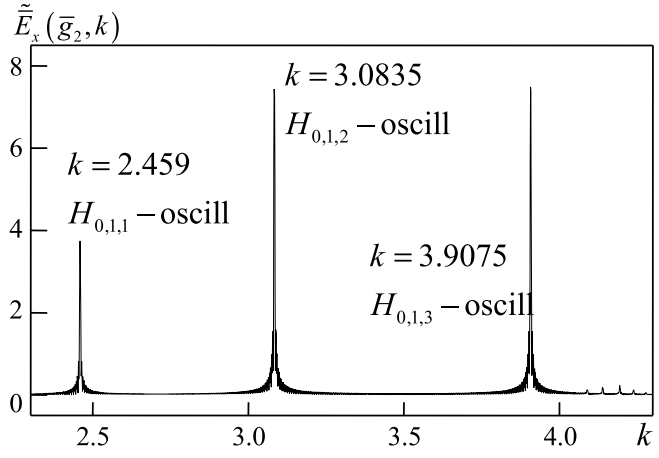

Fig. 10. Real parts of complex wavenumbers defining eigenfrequencies of the storage resonators.

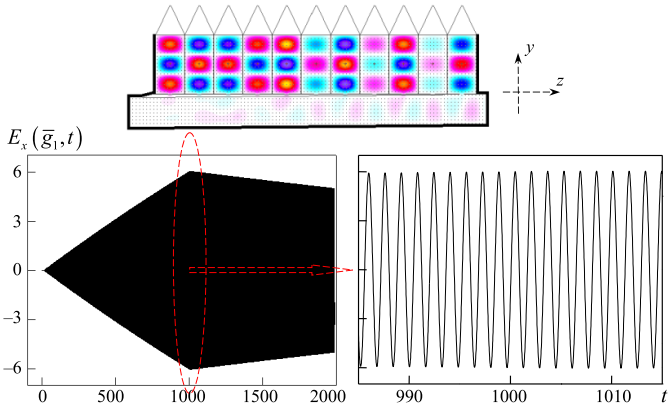

Fig. 11. Excitation of the device by the signal (3) with $\tilde{k} = 3.9075$: field pattern of E_x component and its time signature at the point $\bar{g}_1$, zoom into the vicinity of $t = 1000$.

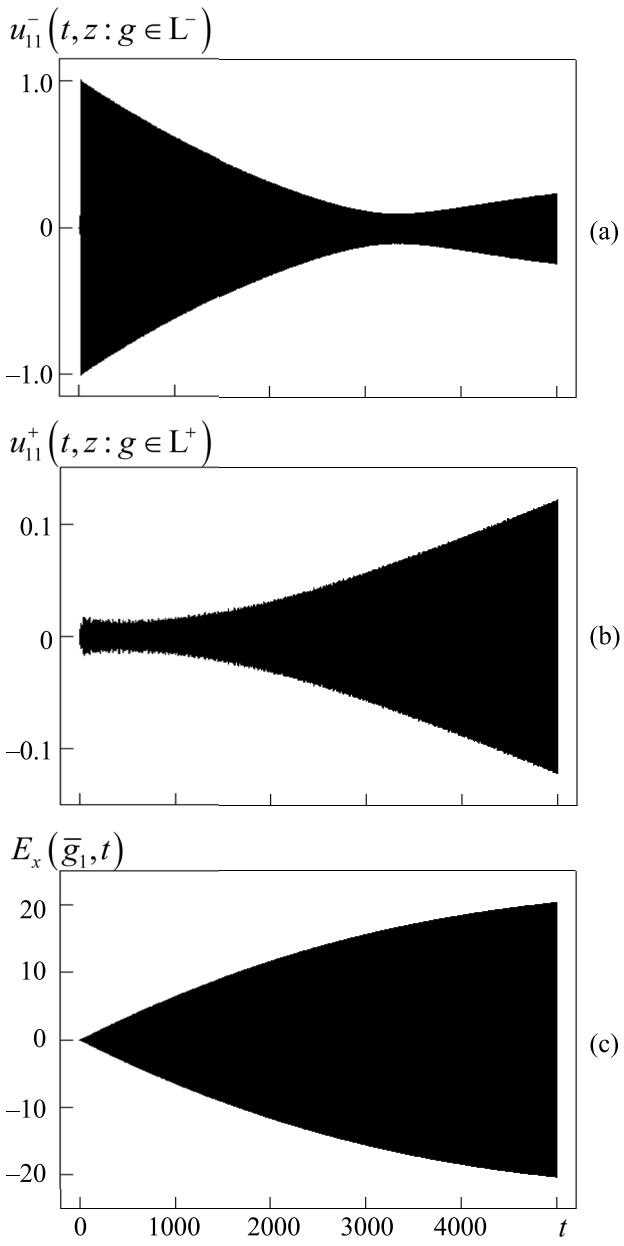

Fig. 12. Energy accumulation mode. Time signatures of the amplitudes of the waves (a) transmitted into B and (b) reflected into A, and (c) field strength at the antinode of the working oscillation.

minus first spatial harmonic of an infinite grating, and the fundamental (zeroth) harmonic is not propagating in this case (see also Section III for details).

The field configuration and the quality factor of the oscillation on the working frequency are determined via exciting the device with the narrowband signal (3) whose parameters are set as $\tilde{k} = \mathrm{Re}\bar{k}_3 \approx 3.9075$, $\tilde{T} = 0.5$, and $P(t) : 0.1 - 5 - 995 - 1000$, see Fig. 11. After switching OFF the source ($t > 1000$), the field of each storage resonator is dominated by the oscillation with complex wavenumber $\bar{k}$. Its real part is set by $\tilde{k}$ of the excitation, and its imaginary part is obtained by studying the envelope of $E_x(\bar{g}_1,t)\chi(t-\tilde{T})\chi(T-t)$, as detailed in Section III. In this case, $\mathrm{Im}\bar{k} \approx -0.00029$. The confident and constant growth of the function $E_x(\bar{g}_1,t)$ until the source is switched OFF (see Fig. 11) indicates the possibility to obtain rather good energy characteristics of the device, as the duration of energy accumulation can be significantly increased without compromising the efficiency.

Setting the duration of energy accumulation as $t_{\mathrm{accum}} = 5000$, we excite the device with the long quasi-monochromatic signal (3) with the following parameters: $\tilde{k} \approx 3.9075$, $\tilde{T} = 0.5$, and $P(t) : 0.1 - 5 - 4995 - 5000$. The characteristics of the device operating in the energy accumulation mode ($0 \le t \le t_{\mathrm{accum}} = 5000$) are presented in Figs. 12 and 13. The coupling between storage resonators on the working frequency and within the considered period of time does not manifest itself—the function $E_x(\bar{g}_1,t)$ grows constantly and its dynamics suggests that the duration of accumulation could be set even longer. The amplitudes reached by the moment of time $t = t_{\mathrm{accum}}$ are almost twice as high as those obtained in Section III, compare Figs. 6(c) and 12(c).

Plots in Fig. 13 are similar to the ones in Fig. 7. Knowing the input energy and its distribution between waveguides A and B [see Fig. 13(a)], we calculate the accumulated (by the moment of time t) energy in the storage

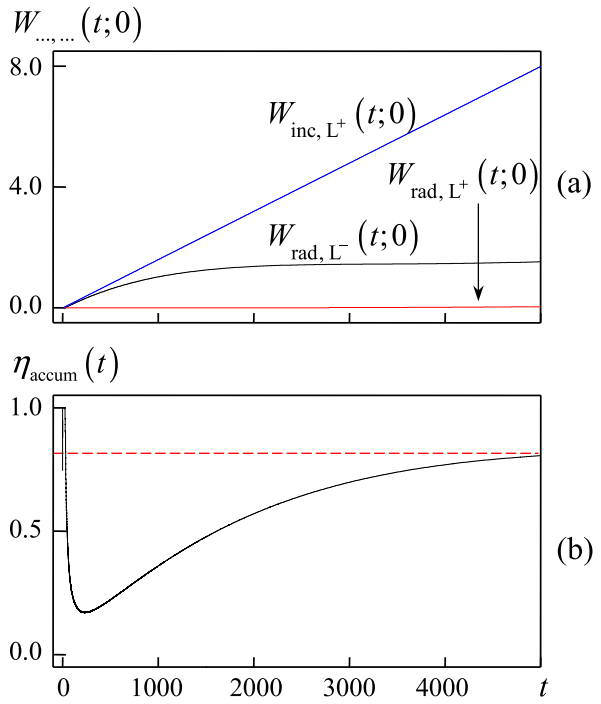

Fig. 13. Energy accumulation mode. (a) Input energy and its distribution between A and B. (b) Accumulation efficiency as functions of time.

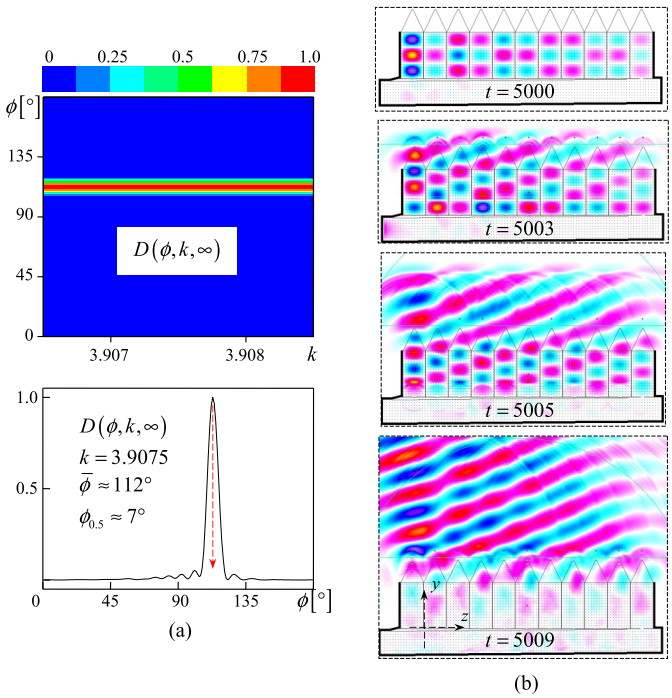

Fig. 15. (a) Far-field radiation patterns for the band and for $k = 3.9075$. (b) Field patterns (E_x component) at various instants of time during the radiation.

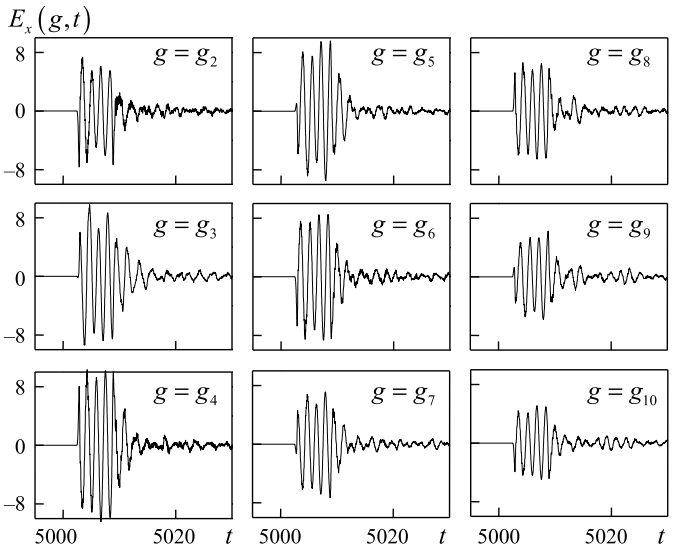

Fig. 14. Time signatures of the radiated pulses at the points g_2–g_{10}.

resonators $W_{\text{accum}}(t;0) = W_{\text{inc, L}^+}(t;0) - W_{\text{rad, L}^+}(t;0) - W_{\text{rad, L}^-}(t;0)$ and the accumulation efficiency $\eta_{\text{accum}}(t) = W_{\text{accum}}(t;0)/W_{\text{inc, L}^+}(t;0)$, see also the discussion of Fig. 7. The plot of $\eta_{\text{accum}}(t)$ [see Fig. 13(b)] indicates that the chosen duration of accumulation $t_{\text{accum}} = 5000$ is close to the optimal as the accumulation efficiency approaches its maximum at this moment of time.

Within the short interval $t_{\text{accum}} = 5000 \le t \le 5001 = t_{\text{rad}}$, the device switches from the energy accumulation mode to the radiation mode and the accumulated energy is released into free space, see Figs. 14 and 15(b). The effective duration of the radiated pulse $\Delta t_{\text{effect}} \approx 10$ and the degree of compression (compression ratio) $\beta = t_{\text{accum}}/\Delta t_{\text{effect}} \approx 500$ are obtained from the time signatures of $E_x(g,t)$ recorded at the points g_1–g_{11} (see Fig. 14), which are located on the line $y = const$ near the peaks of the dielectric screen, as shown in Fig. 9. Knowing the energies in the radiated pulse ($W_{\text{rad, L}}(5050; t_{\text{rad}}) \approx 6.3$) and in the input signal ($W_{\text{inc, L}^+}(t_{\text{accum}}; 0) \approx 8.0$), we calculate the radiation efficiency $\eta_{\text{rad}} = W_{\text{rad, L}}(5050; t_{\text{rad}})/W_{\text{inc, L}^+}(t_{\text{accum}}; 0) \approx 0.788$ and the power amplification factor $\zeta = \beta \cdot \eta_{\text{rad}} \approx 394$. The radiation efficiency is slightly lower than the total accumulation efficiency $\eta_{\text{accum}}(5000) \approx 0.805$, as during the radiation, a fraction of accumulated energy is transmitted (and thus wasted) in waveguides A and B.

Comparing the plots in Figs. 8(a) and 14, we conclude that the efforts to ensure a more uniform distribution of the input energy between the storage resonators turned out to be quite effective. The difference between amplitudes of the waves radiated from the first and last storage resonators is much smaller now. This, in turn, affects the quality of the radiated pulse's wavefront and parameters of the radiation pattern, see Fig. 15. The far-field radiation pattern has only one lobe, and it is narrower now. The orientation of the main lobe ($\bar{\phi} \approx 112^\circ$) perfectly matches the theoretically predicted one ($\bar{\phi} \approx 111.5^\circ$). This once again confirms the correctness of the design approach and modeling of the proposed device.

The wavenumber 3.9075 [rad/m] corresponds to the working frequency ≈ 186.44 MHz. To be used in plasma heating applications, the working frequency should be 20–1000 times higher [7]. The obtained results are scalable with ease to any geometrically similar devices. For it, all parameters bearing the

dimension [m] (e.g., geometry parameters) should be multiplied by the corresponding similarity factor, and all parameters bearing the dimension [m^{-1}] (e.g., wavenumbers) should be divided by it.

We would like to note that we have presented not a real-world device, but a model aiming to demonstrate the new method for formation and directional radiation of short and powerful pulses and its development steps. The switching between energy accumulation and radiation modes is briefly touched, and the utilized switch is an "ideal" model. Designing real-world device, one should keep in mind the importance of thoughtful selection of the switch type and carefully tuning its parameters. The characteristics of the switch drastically affect the characteristics of the whole device [1], [3], [4]. This topic lies beyond the paper's scope, but we think that the most suitable options for the presented devices are gas discharge switches or switches triggered via electron injection [3]. The latter ones switch faster between open and closed states and thus are preferred.

V. Conclusion

The presented results demonstrate and prove that finite periodic structures composed of sufficiently high-quality resonators are capable to form and directionally radiate short and powerful pulses. A fairly well-grounded assumption about such an option had been made in [34]. Now, this assumption is confirmed by specific data obtained in experiments with rigorous models of the method of EACs, which provide accurate analysis of complex electrodynamic structures under conditions of possible resonant scattering of waves. In the functional scheme of the considered prototype of the device, it is easy to find elements inherent in phased array antennas, diffraction radiation (leaky-wave) antennas, and active compressors of EM pulses. Therefore, the results presented here were, of course, inspired by the results of many researchers working in the relevant directions.

These results were obtained in computational experiments with simple models, which allow to study and understand features of the processes of energy accumulation, formation, and directional radiation of short and powerful radio pulses. Perfect understanding of these processes is a milestone for real-world devices. Using simple and easy to understand models, such studies could be accomplished without reference to details of a specific device or its active elements. It is assumed that all functionally significant features are included in design models at the optimization stage.

Appendix

This details EACs, transition to frequency domain, and the device's characteristics available for analysis.

A. EACs Explained

EACs $D^+[E_x(g,t)-V_p(g,t)]|_{g\in \mathrm{L}^+}=0$, $D^-[E_x(g,t)]|_{g\in \mathrm{L}^-}=0$, and $D[E_x(g,t)]|_{g\in \mathrm{L}}=0$ for the virtual boundaries L^+, L^-, and L [see problem (1) and Fig. 1] provide an ideal model for the outgoing (from the computation domain Ω_{int} into the waveguides A, B, and the domain Ω_{ext}) waves, which are defined as follows:

$$\begin{aligned} &E_x(g,t)-V_p(g,t)\\ &\quad=\sum_{n=1}^{\infty}u_{np}^{+}(z,t)\mu_n(y);\quad g\in\bar{A},\quad t\geq 0,\\ &E_x(g,t)=\sum_{n=1}^{\infty}u_{np}^{-}(z,t)\mu_n(y);\quad g\in\bar{B},\quad t\geq 0,\quad \text{and}\\ &E_x(g,t)=\sum_{m=-\infty}^{\infty}u_{mp}(\rho,t)\bar{\mu}_m(\phi);\quad \rho\geq R,\quad 0\leq\phi\leq 2\pi,\\ &\qquad\qquad t\geq 0. \end{aligned} \tag{A1}$$

The outgoing waves (A1) pass through the virtual boundaries with EACs imposed without any reflection or distortion, as if they are absorbed by these boundaries or the domain Ω_{ext}.

The operators $D^{\pm}[\ldots]$, $D[\ldots]$ and the orthonormal systems of complete transverse functions $\{\mu_n(y)\}_{n=1}^{\infty}$, $\{\bar{\mu}_m(\phi)\}_{m=-\infty}^{\infty}$ are defined in [4], [21], and [22]. The space-time amplitudes $u_{np}^{\pm}(z,t)$ and $u_{mp}(\rho,t)$ on the virtual boundaries $\mathrm{L}^{\pm}$ and C_R are determined from the solution to problem (1). The values $u_{mp}(\rho,t)$ for $\rho>R$ (outside C_R), which are necessary for calculating far-field characteristics, are obtained from the values $u_{mp}(R,t)$ (on C_R) using the transport operators, which are detailed in [22] and [25].

B. Transition to Frequency Domain

When problem (1) is solved and the function $E_x(g,t)$ is obtained for $g\in\overline{\Omega_{\text{int}}}\cup\Omega_{\text{ext}}$ and all time moments $t\in[0,T]$, $T<\infty$, the transition to frequency domain is carried out using the integral transform

$$\tilde{f}(k)=\int_0^T f(t)\exp(ikt)dt. \tag{A2}$$

Here, T is the upper time limit of the observation interval $[0,T]$, $k=2\pi/\lambda>0$ is a wavenumber, and λ is a wavelength in free space; for all $t>T$, the function $f(t)$ undergoing the transformation is set to zero. As it was mentioned in the end of Section I, in this article, we use wavenumber as a frequency parameter. Thus, all frequency-domain characteristics exhibit dependence on k.

C. Characteristics for Analysis

The following characteristics are available for the analysis of the physics of processes [3], [4], [8], [18], [24].

1) Field patterns of $E_x(g,t)$, $g\in\overline{\Omega_{\text{int}}}$ and other components of EM field, both at any fixed moment of time $t\in[0,T]$ and within any finite time interval $[t_1,t_2]\in[0,T]$, in the form of a corresponding dynamic picture. Other nonzero components of the field are defined by the following relations: $\partial_t H_y(g,t)=-\eta_0^{-1}\partial_z E_x(g,t)$ and $\partial_t H_z(g,t)=\eta_0^{-1}\partial_y E_x(g,t)$.
2) Space-time amplitudes $u_{np}^{\pm}(z,t)$ and $u_{mp}(\rho,t)$ of the waves (A1) on the virtual boundaries $\mathrm{L}^{\pm}$ and C_R within any finite time interval $[t_1,t_2]\in[0,T]$.
3) Input energy $W_{\text{inc, L}^+}(t_2;t_1)$ (incomes from A through L^+) and radiated energies $W_{\text{rad, L}^{\pm}}(t_2;t_1)$ (transmitted

through L^+ or L^- into A or B) and $W_{\text{rad, L}}(t_2; t_1)$ (radiated through L into Ω_{ext}), all within a certain period of time $t_1 \le t \le t_2$. These energies are determined by integrating over t the instantaneous powers passing through the corresponding boundaries within the interval $t_1 \le t \le t_2$.

4) Field patterns of components of the frequency-domain field $\{\tilde{\boldsymbol{E}}(g,k), \tilde{\boldsymbol{H}}(g,k)\}$, $g \in \overline{\Omega_{\text{int}}}$.
5) $R_{np}(k)$ and $T_{np}(k)$, which are the transformation coefficients of incoming (from A) TE_{0p}-wave into TE_{0n}-waves reflected back into A and transmitted into B, respectively.
6) $\eta(k) = 1 - W_{\text{abs}}(k) - \sum_n [W_{np}^+(k) + W_{np}^-(k)]$, which is the efficiency of transformation of the excitation wave into the radiation field.
7) $D(\phi, k, M) = \frac{|\tilde{E}_{\text{tg}}(M,\phi,k)|^2}{\max\limits_{\Phi_1 \le \phi \le \Phi_2} |\tilde{E}_{\text{tg}}(M,\phi,k)|^2}$, $K_1 \le k \le K_2$, $0 \le \Phi_1 \le \phi \le \Phi_2 \le 360°$, which is the normalized radiation pattern calculated on the arc $\rho = M \ge R$.
8) Angle $\phi = \bar{\phi}(k)$ which determines the orientation of the main lobe: $D(\bar{\phi}(k), k, M) = 1.0$.
9) Half-power beamwidth $\phi_{0.5}(k)$: $\phi_{0.5}(k) = \phi^+ - \phi^-$, $\bar{\phi} \in [\phi^-, \phi^+]$, where $D(\phi^+, k, M) = 0.5$ and $D(\phi^-, k, M) = 0.5$.

Here, $\tilde{\boldsymbol{E}}_{\text{tg}}(M, \phi, k)$ is the tangential component of the frequency-domain electric field on the circle $\rho = M \ge R$; $W_{\text{abs}}(k)$ is a portion of the energy absorbed in imperfect dielectrics; and $W_{np}^-(k)$ and $W_{np}^+(k)$ are portions of the energy transmitted and reflected through the virtual boundaries L^- and L^+ into the waveguides B and A, respectively. In the framework of the model problem (1), not only the function $\eta(k)$ is calculated but also its components $W_{\text{abs}}(k)$, $W_{np}^-(k)$, and $W_{np}^+(k)$. This information allows to identify and analyze separately such important characteristics as the radiation efficiency, the matching level of feeders with radiating element, the conversion efficiency of dielectric waveguide surface waves into radiation field. To calculate the far-field radiation pattern $D(\phi, k, \infty)$, which is used most in this article, the values of $\tilde{\boldsymbol{E}}_{\text{tg}}(\infty, \phi, k)$ are required. They are obtained from the corresponding entities on the virtual boundary C_R using the transform (A2) and the transport operators [22], [25] or as explained in [4, Ch. 5].

ACKNOWLEDGMENT

The authors would like to thank their friend and colleague Vadym Pazynin for his valuable comments on switches.

REFERENCES

[1] C. E. Baum, "Options in microwave pulse compression," *Circuit Electromagn. Syst. Des. Notes*, no. 68, May 2010.
[2] A. D. Andreev, E. G. Farr, and E. Schamiloglu, "A simplified theory of microwave pulse compression," *Circuit Electromagn. Syst. Des. Notes*, no. 57, Aug. 2008.
[3] K. Sirenko, V. Pazynin, Y. Sirenko, and H. Bagci, "Compression and radiation of high-power short RF pulses. I. Energy accumulation in direct-flow waveguide compressors," *Prog. Electromagn. Res.*, vol. 116, pp. 239–270, 2011, doi: 10.2528/PIER11022003.
[4] Y. Sirenko and L. Velychko, Eds., *Electromagnetic Waves in Complex Systems: Selected Theoretical and Applied Problems*. Berlin, Germany: Springer, 2016, doi: 10.1007/978-3-319-31631-4.
[5] V. L. Bratman *et al.*, "Generation of 3 GW microwave pulses in X-band from a combination of a relativistic backward-wave oscillator and a helical-waveguide compressor," *Phys. Plasmas*, vol. 17, no. 11, Nov. 2010, Art. no. 110703, doi: 10.1063/1.3505825.
[6] V. L. Pazynin and M. V. Maiboroda, "Compression of electromagnetic pulses in an asymmetric dielectric waveguide," *Telecommun. Radio Eng.*, vol. 78, no. 2, pp. 97–107, 2019, doi: 10.1615/TelecomRadEng.v78.i2.10.
[7] J. Benford, J. A. Swegle, and E. Schamiloglou, *High Power Microwaves*, 3rd ed. Boca Raton, FL, USA: CRC Press, 2016.
[8] K. Sirenko, V. Pazynin, Y. K. Sirenko, and H. Bağci, "Compression and radiation of high-power short RF pulses. II. A novel antenna array design with combined compressor/radiator elements," *Prog. Electromagn. Res.*, vol. 116, pp. 271–296, 2011, doi: 10.2528/PIER11022004.
[9] S. Smith and E. M. Purcell, "Visible light from localized surface charges moving across a grating," *Phys. Rev.*, vol. 92, no. 4, pp. 1069–1073, Nov. 1953, doi: 10.1103/PhysRev.92.1069.
[10] V. P. Shestopalov, *The Smith-Purcell Effect*. New York, NY, USA: Nova Science, 1998.
[11] S. Sautbekov, K. Sirenko, Y. Sirenko, and A. Yevdokymov, "Diffraction radiation effects: A theoretical and experimental study," *IEEE Antennas Propag. Mag.*, vol. 57, no. 5, pp. 73–93, Oct. 2015, doi: 10.1109/MAP.2015.2470673.
[12] Y. Sirenko, S. S. Sautbekov, N. Yashina, and K. Sirenko, "Diffraction radiation generated by a density-modulated electron beam flying over the periodic boundary of the medium section. I. Analytical basis," *Prog. Electromagn. Res. B*, vol. 91, pp. 1–8, 2021, doi: 10.2528/PIERB20110105.
[13] K. Y. Sirenko, Y. K. Sirenko, and A. P. Yevdokymov, "Diffraction antennas. A ridged dielectric wavegide," *Telecommun. Radio Eng.*, vol. 77, no. 10, pp. 839–852, 2018, doi: 10.1615/TelecomRadEng.v77.i10.10.
[14] S. S. Sautbekov, K. Y. Sirenko, Y. K. Sirenko, and A. P. Yevdokymov, "Diffraction antennas. Synthesis of radiating elements," *Telecommun. Radio Eng.*, vol. 77, no. 11, pp. 925–943, 2018, doi: 10.1615/TelecomRadEng.v77.i11.10.
[15] Y. K. Sirenko and A. P. Yevdokymov, "Diffraction antennas. Linear structures on the basis of a ridged dielectric waveguide," *Telecommun. Radio Eng.*, vol. 77, no. 14, pp. 1203–1229, 2018, doi: 10.1615/TelecomRadEng.v77.i14.10.
[16] V. Z. Mazur, K. Y. Sirenko, Y. K. Sirenko, and A. P. Yevdokymov, "Diffraction antennas. Linear structures on the basis of a modified Goubau line," *Telecommun. Radio Eng.*, vol. 77, no. 16, pp. 1397–1408, 2018, doi: 10.1615/TelecomRadEng.v77.i16.10.
[17] K. Y. Sirenko, Y. K. Sirenko, and A. P. Yevdokymov, "Diffraction antennas. Planar structures with controllable beam positioning," *Telecommun. Radio Eng.*, vol. 78, no. 10, pp. 835–851, 2019, doi: 10.1615/TelecomRadEng.v78.i10.10.
[18] I. K. Kuzmitchev *et al.*, "Model synthesis of energy compressors," *Radiofizika i Elektronika*, vol. 13, no. 2, pp. 166–172, 2008.
[19] N. Burambayeva, S. Sautbekov, Y. K. Sirenko, and A. Vertiy, "Compact open resonator as the power-storage unit for a microwave compressor," *Telecommun. Radio Eng.*, vol. 74, no. 1, pp. 29–40, 2015, doi: 10.1615/TelecomRadEng.v74.i1.30.
[20] P. N. Melezhik and Y. K. Sirenko, "New type of storage resonator for an electromagnetic pulse compressor," *J. Commun. Technol. Electron.*, vol. 65, no. 4, pp. 355–366, Apr. 2020, doi: 10.1134/S1064226920040051.
[21] K. Sirenko and Y. Sirenko, "Exact 'absorbing' conditions in the initial boundary value problems of the theory of open waveguide resonators," *Comput. Math. Math. Phys.*, vol. 45, no. 3, pp. 490–506, 2005.
[22] Y. Sirenko, S. Strom, and N. Yashina, *Modeling and Analysis of Transient Processes in Open Resonant Structures: New Methods and Techniques*. New York, NY, USA: Springer, 2007, doi: 10.1007/0-387-32577-8.
[23] Y. Sirenko, V. Pazynin, K. Sirenko, and N. Yashina, "Exact absorbing conditions for initial boundary value problems of computational electrodynamics. Review," in *A Closer Look at Boundary Value Problems*, M. Avci, Ed. New York, NY, USA: Nova Science, 2020, pp. 43–124.
[24] Y. Sirenko and S. Strom, Eds., *Modern Theory of Gratings. Resonant Scattering: Analysis Techniques and Phenomena*. New York, NY, USA: Springer, 2010, doi: 10.1007/978-1-4419-1200-8.
[25] K. Sirenko, V. Pazynin, Y. K. Sirenko, and H. Bagci, "An FFT-accelerated FDTD scheme with exact absorbing conditions for characterizing axially symmetric resonant structures," *Prog. Electromagn. Res.*, vol. 111, pp. 331–364, 2011, doi: 10.2528/PIER10102707.

[26] K. Sirenko, M. Liu, and H. Bagci, "Incorporation of exact boundary conditions into a discontinuous Galerkin finite element method for accurately solving 2D time-dependent Maxwell equations," *IEEE Trans. Antennas Propag.*, vol. 61, no. 1, pp. 472–477, Jan. 2013, doi: 10.1109/TAP.2012.2220102.

[27] Y. K. Sirenko, L. G. Velychko, and F. Erden, "Time-domain and frequency-domain methods combined in the study of open resonance structures of complex geometry," *Prog. Electromagn. Res.*, vol. 44, pp. 57–79, 2004, doi: 10.2528/PIER03030601.

[28] L. G. Velychko, Y. K. Sirenko, and O. S. Velychko, "Time-domain analysis of open resonators. Analytical grounds," *Prog. Electromagn. Res.*, vol. 61, pp. 1–26, 2006, doi: 10.2528/PIER06020701.

[29] L. G. Velychko and Y. K. Sirenko, "Controlled changes in spectra of open quasi-optical resonators," *Prog. Electromagn. Res. B*, vol. 16, pp. 85–105, 2009, doi: 10.2528/PIERB09060202.

[30] M. Neviere and E. Popov, *Light Propagation in Periodic Media: Differential Theory and Design*. Boca Raton, FL, USA: CRC Press, 2003, doi: 10.1201/9781482275919.

[31] R. Petit, Ed., *Electromagnetic Theory of Gratings*. Berlin, Germany: Springer, 1980, doi: 10.1007/978-3-642-81500-3.

[32] V. Shestopalov, A. Kirilenko, S. Masalov, and Y. Sirenko, *Resonance Wave Scattering: Diffraction Gratings*, vol. 1. Kyiv, Ukraine: Naukova Dumka, 1986.

[33] V. Shestopalov and Y. Sirenko, *Dynamic Theory of Gratings*. Kyiv, Ukraine: Naukova Dumka, 1989.

[34] S. S. Sautbekov, K. Y. Sirenko, Y. K. Sirenko, A. Y. Poyedinchuk, N. P. Yashina, and A. P. Yevdokymov, "The Smith–Purcell effect. Anomalously high level of outgoing wave excitation," *Telecommun. Radio Eng.*, vol. 77, no. 6, pp. 469–487, 2018, doi: 10.1615/TelecomRadEng.v77.i6.10.

Yuriy Sirenko received the M.S. degree in calculus mathematics, the Ph.D. degree in physics and mathematics, and the D.Sc. degree in physics and mathematics from V.M. Karazin Kharkiv National University, Kharkiv, Ukraine, in 1971, 1978, and 1988, respectively.

From 2013 to 2017, he was an Invited Professor with L.N. Gumilyov Eurasian National University, Astana, Kazakhstan. Since 1974, he sequentially held a number of academic and administrative positions with the O.Ya. Usikov Institute for Radiophysics and Electronics NASU, Kharkiv, where he has been a Chief Researcher since 2016. He has authored or coauthored ten books and more than 200 journal papers. His current research interests include wave scattering theory, analytical and numerical techniques for wave motion simulation, resonance phenomena, spectral theory of open structures, operator theory, and its applications.

Prof. Sirenko was a recipient of the State Prize of Ukraine in Science and Technology in 1989.

Seil Sautbekov received the M.S. degree in physics and the Ph.D. degree in physics and mathematics from Al-Farabi Kazakh National University (KNU), Almaty, Kazakhstan, in 1977 and 1987, respectively, and the D.Sc. degree in physics and mathematics with specialization in radiophysics from the Kotelnikov Institute of Radio-Engineering and Electronics RAS, Moscow, Russia, in 2002.

From 1985 to 2004, he held several research and academic positions with KNU. From 2004 to 2018, he was a Professor with L.N. Gumilyov Eurasian National University, Astana, Kazakhstan. He is currently a Research Professor with KNU. He is well-known expert in the theory of electromagnetic (EM) wave propagation in anisotropic media. He has expertise in the applications of the factorization method for solving singular integral equations. He has authored or coauthored over 100 scientific publications.

Prof. Sautbekov received the title "Best Lecturer in Higher Education of Kazakhstan" in 2007 and award for his contribution to the Development of Sciences of the Republic of Kazakhstan in 2010.

Nataliya Yashina received the M.S. degree (*cum laude*) and the Ph.D. degree in radiophysics from V.M. Karazin Kharkiv National University, Kharkiv, Ukraine, in 1973 and 1979, respectively, and the Diploma HDR from Blaise Pascal University, Clermont-Ferrand, France, in 2003.

She is currently a Senior Researcher with the O.Ya. Usikov Institute for Radiophysics and Electronics NASU, Kharkiv. She has authored or coauthored three books and over 100 journal and conference papers published in Russian, English, and French. Her current research interests include accurate numerical modeling of complicated and resonant processes in compound dispersive structures.

Dr. Yashina received the title of Senior Scientist from the National Academy of Sciences of Ukraine in 1996.

Kostyantyn Sirenko (Member, IEEE) received the M.S. degree in mathematics and informatics from V.N. Karazin Kharkiv National University, Kharkiv, Ukraine, in 2004, and the Ph.D. degree in physics and mathematics from the O.Ya. Usikov Institute for Radiophysics and Electronics NASU, Kharkiv, in 2008.

From 2008 to 2014, he held a post-doctoral position with Blaise Pascal University, Clermont-Ferrand, France, and the King Abdullah University of Science and Technology (KAUST), Thuwal, Saudi Arabia. Since 2014, he has been in the private sector as a Scientific and Technical Consultant, and collaborates sometimes with his colleagues from O.Ya. Usikov Institute. He has authored or coauthored three book chapters and more than 30 journal articles. His current research interests include numerical analysis, electromagnetics (EMs) simulations, and microwave energy compressors.

Dr. Sirenko received the Young Scientist Award at the URSI EMTS Symposium in 2010.